tration. The slope of this line, $-(\Delta\gamma/\Delta c)_{Tc=0-0.1M}$, is considered to be proportional to the surface accumulation, Γ, (described by the Gibbs equation) and thus to reflect the hydrophobicity of the water-soluble α-amino acids.

Crystal Structure Determinations. Crystals of optically pure phenylalanine, *tert*-butylglycine, neopentylglycine, and racemic *tert*-butylglycine and hexafluorovaline were grown by slow evaporation from their aqueous solutions as plates. Cell dimensions and X-ray intensity measurements were performed on a rotating anode Rigaku diffractometer using Cu or Mo Kα radiations. The space groups of all the systems were unequivocally determined (Table I). The crystal structures were solved by use of the SHELX-86 and refined by SHELX-76 programs.[24] The X-ray structure refinements of all the crystals were satisfactory but for phenylanaline. Their agreement factors R(F) varied from 0.04 to 0.069 (Table IV). The bond lengths, bond angles, temperature factors, and intermolecular distances were normal, indicating correct structure determination (available as supplementary material). The structure of optically pure phenylalanine, with two molecules per asymmetric unit, was refined to a R(F) value of 0.147. There is also too short a H···H distance of 1.8 Å between the hydrogen atoms of neighboring phenyl rings related by translation along the b axis (Figure 3c). The carbon atoms of the two independent phenyl rings show unusually large displacement parameters $U_{ii}(i = 1,3)$, as high as 0.25 Å^2, for the C(5), C(6), (C8), and C(9) (or C(52), C(62), C(82) and C(92)) atoms. We interpret these results in terms of orientational disorder of the phenyl rings: The short 1.8 Å contact may be increased to an acceptable value of 2.2 Å by rotating the phenyl rings by 15° about the C(4)–C(7) (or C(42)–C(72)) axis. The rotation may be clockwise or counterclockwise, but the direction of rotation will be the same for a row of molecules related by transition along the b axis. This would lead to abnormally high displacement parameters for the phenyl ring atoms and the "short" 1.8 Å H···H separation, since the structure was refined with only one phenyl ring per molecule. This proposed disorder of the phenyl rings does not cast doubt on the correctness of the overall packing arrangement and on the hydrogen-bonding structure which is our primary interest.

(24) Sheldrick, G. M. *SHELX-86 Program for Crystal Structure Determination*; Cambridge University: Cambridge, England, 1986; *SHELX-76 Program*; Cambridge University: Cambridge, England, 1976.

Acknowledgment. We thank the Minerva Foundation, the Israel Academy of Science and Humanities and the U.S./Israel Binational Science Foundation, Jerusalem, for financial support. We thank Dr. Karlheintz Drauz from the Degussa Company for kindly supplying of *tert*-butylglycine and neopentylglycine.

Supplementary Material Available: Tables of crystal data, atomic coordinates, anisotropic temperature factors, hydrogen atom coordinates and isotropic temperature factors, bond lengths, and bond angles for (*S*)-neopentylglycine, (*S*)-*tert*-butylglycine, (*RS*)-hexafluorovaline, and (*R*)-phenylalanine (47 pages). Ordering information is given on any current masthead page.

Dynamics of Two-Dimensional Self-Aggregation: Pressure and pH-Induced Structural Changes in a Fluorocarbon Amphiphile at Liquid–Air Interfaces. An X-ray Synchrotron Study

D. Jacquemain,[†] S. Grayer Wolf,[†] F. Leveiller,[†] M. Lahav,[†] L. Leiserowitz,*[,†] M. Deutsch,[‡] K. Kjaer,[§] and J. Als-Nielsen*[,§]

Contribution from the Structural Chemistry Department, Weizmann Institute of Science, Rehovot 76100, Israel, Physics Department, Bar-Ilan University, Ramat-Gan 52100, Israel, and Physics Department, Risø National Laboratory, DK4000 Roskilde, Denmark.
Received January 31, 1990

Abstract: In order to provide, on the molecular level, information on crystal nucleation of monolayers at air–water interfaces, the self-aggregation of 1H,1H,2H,2H-perfluorododecyl aspartate $CF_3(CF_2)_9(CH_2)_2OCOCH_2CH(NH_3^+)CO_2^-$ (PFA) over water subphases at various pH values was studied using synchrotron X-ray grazing incidence diffraction (GID), including Bragg rods (BR) and reflectivity (XR) measurements. Two-dimensional crystalline domains with coherence lengths exceeding 1500 Å were detected for low surfactant surface densities and zero surface pressure. GID measurements reveal structural changes with subphase pH and composition. Structural models are proposed at high, neutral, and low pH. For water subphases containing KOH at pH ≥ 11.2, the diffraction is consistent with molecules arranged in a hexagonal net and vertically aligned. Over pure water and acidic subphases containing HCl at pH = 1.5, the molecules pack in a distorted hexagonal net with the fluorocarbon chains tilted from the vertical. The growth in time of the uncompressed crystallites over aqueous glycine solutions was directly monitored by GID. Compression and subsequent decompression of the monolayers over pure water and HCl (pH = 1.5) subphases, for which the fluorocarbon chains are originally tilted, were found to reduce the crystallinity of the system considerably. By contrast, over KOH at pH ≥ 11.2, the hexagonal net with vertically aligned molecules is preserved at all surface pressures and the crystalline order of the system is reduced upon compression but increases again upon release of pressure. Estimates of the degree of crystallinity of the monolayer were made over water for various states of compression and over KOH at pH ≥ 11.2 in the uncompressed state. The packing characteristics and the dynamics involved in the formation and partial destruction of the crystallites can be understood in terms of interaction between the hydrophilic ionic head groups of the monolayer and, if present, the attached molecules or ions (water, K^+ or Cl^-). Additional support for the packing arrangements proposed at high, neutral, and low pH was obtained from studies of the oriented growth of sodium chloride under PFA monolayers.

1. Introduction

Our understanding of the mechanisms of crystal nucleation and growth on a molecular level is still at a rudimentary stage. Direct observation of three-dimensional (3-D) nucleation processes in solution is extremely difficult. Earlier work carried out on the oriented growth of α-glycine[1] crystals at interfaces from aqueous solutions in the presence of dissolved short-chain hydrophobic α-amino acids,[2] indicates that the α-amino acids form structured

[†] Weizmann Institute of Science.
[‡] Bar-Ilan University.
[§] Risø National Laboratory.

(1) Glycine is known to crystallize in three different forms α, β, and γ-glycine. The α form is the most common one, which we refer to as "glycine" throughout the paper.

0002-7863/90/1512-7724$02.50/0

two-dimensional (2-D) aggregates at the interface, which function as nucleating centers for the crystallization of glycine. However, X-ray diffraction techniques were not sensitive enough to allow for the direct identification of these aggregates.

By extension, amphiphilic α-amino acids that form Langmuir monolayers were designed for the promotion of glycine crystallization at air–solution interfaces.[3a,b] Recently developed synchrotron X-ray surface techniques provided new tools to determine the 2-D crystalline structure of these compressed α-amino acid monolayers.[4a,5] The structural determination of compressed palmitoyllysine (PL) from grazing incidence X-ray diffraction[4]

$$CH_3(CH_2)_{14}CONH(CH_2)_4CH(NH_3^+)CO_2^- \text{ (PL)}$$

(GID) and X-ray specular reflectivity[6] (XR) measurements showed unambiguously that an excellent structural match existed between the packing arrangement of the α-amino acid head-groups of PL and the glycine layers in the growing 3-D crystal.[4a,7]

Remarkably, when the average surface density of PL is one tenth that of the fully compressed monolayer, glycine crystals still grow in an oriented way from the interface.[3b,c] In keeping with the results observed for the short-chain hydrophobic α-amino acids, we proposed that this result provided evidence that PL molecules self-assemble at the air–solution interface to yield structured aggregates. However, attempts to detect such clusters for noncompressed monolayers of PL at room temperature by GID have proven unsuccessful as yet; the diffraction peaks observed for the compressed monolayer disappeared upon reduction of surface pressure below 10 mN/m.[4a,7]

Fluorocarbon chains have several distinct advantages over hydrocarbon chains. The higher X-ray scattering power of the fluorine atom relative to hydrogen enhances GID detectability. Furthermore, the fluorine atoms, which induce a helical conformation in long fluorocarbon chains, render them stiffer than aliphatic hydrocarbon chains and lower the possibility for conformational disorder. The fluorocarbon 1H,1H,2H,2H-perfluorododecyl aspartate (PFA) was designed, as was PL, to be

$$CF_3(CF_2)_9(CH_2)_2OCOCH_2CH(NH_3^+)CO_2^- \text{ (PFA)}$$

used as a monolayer for the promotion of oriented crystallization at the interface. The crystalline structure of compressed PFA monolayers as determined by GID and XR measurements[5] showed some measure of mismatch between the layer arrangement of the α-amino acid moieties of the monolayer and the layered crystal structure of glycine. Nevertheless, PFA still induced formation of glycine crystals from specific faces at the interface, even when noncompressed.[3b,c]

Unlike for PL, we report here for PFA the detection by GID of *crystalline self-clustering* for low-surface densities of the surfactant and zero surface pressure. We show that the molecular packing and orientation in the formed crystalline clusters (crystallites) is a function of the subphase pH and composition. The molecular-packing characteristics in the crystallites are interpreted in terms of interactions between the hydrophilic ionic head-groups of PFA and, if present in the solution subphase, the attached molecules or ions. We also present results concerning the dynamics of the system. For the first time, we could directly monitor *on a molecular level the growth of the crystallites in time* by using GID. The behavior of the PFA crystallites upon compression and decompression is also studied in detail and shown to be dependent on the original molecular packing and orientation. Finally, we use the complementary technique of oriented growth of NaCl crystals underneath monolayers of PFA as an independent probe of the interfacial structure[3d] at high, neutral, and low pH.

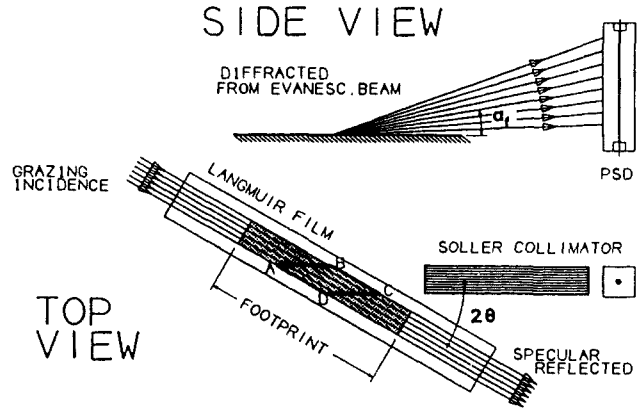

Figure 1. Top and side views of the GID geometry. The footprint of the grazing incidence beam is indicated by the darker area. The position sensitive detector (PSD) has its axis along the vertical direction (z). Only the area ABCD contributes to the scattering.

2. Experimental Section

Materials. PFA chemical purity was determined by elemental analysis, NMR, and IR spectroscopies; enantiomeric purity was measured by GC analyses on a gas chromatograph equipped with a Chirasil-L-Valine column.[3b] Spreading solutions of PFA were prepared in chloroform (Merck, analytical grade)/trifluoroacetic acid (Aldrich, spectrophotometric grade) 96/4 (v/v). The water used was purified by using a Millipore system (pH = 5.8). The subphase composition and pH were varied in some measurements with 37% HCl (Merck, analytical grade), NaOH and KOH in pellets (Merck, analytical grade), CsOH (Aldrich, purity 99.9%), or glycine (BDH, >99%). NaCl crystallizations under PFA monolayers were carried out in a thermostated circular trough at 20 ± 0.1 °C by spreading PFA solutions over supersaturated aqueous solution of NaCl (5.66 M, Merck, analytical grade).[3c]

Monolayer Experiments. The X-ray measurements on PFA monolayers were carried out by using the liquid surface diffractometer on beam line D4 at Hasylab, DESY, Hamburg. A sealed and thermostated Langmuir trough equipped with a Wilhelmy balance was mounted on the diffractometer. The temperature in the trough was 20 ± 0.1 °C. For the GID measurements, detection was made by a linear position sensitive dectector (PSD) mounted vertically behind a horizontally collimating Soller slit (Figure 1) of resolution $\Delta(2\theta) = 1.5$ mrad (full width at half maximum (fwhm)). For a measured diffraction peak of width fwhm(2θ), the resolution corrected width is $W = [\text{fwhm}(2\theta)^2 - \Delta(2\theta)^2]^{1/2}$. By the Debye–Scherrer formula,[8] this corresponds to a coherence length of $L = 0.90\lambda/(W \cos\theta)$, where $\lambda = 1.38$ Å is the wavelength used. Since the finite height of the PSD corresponds to a measuring window of $\Delta q_z = 0.33$ Å^{-1} ($\bar{q}_z$ is the component of the scattering vector in the z direction, $q_z = (2\pi/\lambda) \sin\alpha_f$), in GID experiments the observed intensity is integrated over a finite q_z slice of a Bragg rod (BR, see section 3). It was therefore sometimes necessary to shift the PSD in the $\bar{q}_z$ vertical direction to obtain a full measurement of a given BR. The GID angle of incidence was $0.85\alpha_c$, where $\alpha_c = 0.138°$ is the critical angle for total external reflection. The dimensions of the footprint of the incoming X-ray beam on the surface were 50 × 5 mm. For XR measurements the PSD was substituted by a scintillation detector subtending 0.13° in α_f (Figure 1). Further details are given elsewhere.[4a,5,7]

(2) Weissbuch, I.; Addadi, L.; Berkovitch-Yellin, Z.; Gati, E.; Lahav, M.; Leiserowitz, L. *Nature* **1984**, *310*, 161–164.
(3) (a) Landau, E. M.; Levanon, M.; Leiserowitz, L.; Lahav, M.; Sagiv, J. *Nature*, **1985**, *318*, 353–356. (b) Landau, E. M.; Grayer Wolf, S.; Levanon, M.; Leiserowitz, L.; Lahav, M.; Sagiv, J. *J. Am. Chem. Soc.* **1989**, *111*, 1436–1445. (c) Landau, E. M.; Grayer Wolf, S.; Sagiv, J.; Deutsch, M.; Kjaer, K.; Als-Nielsen, J.; Leiserowitz, L.; Lahav, M. *Pure Appl. Chem.* **1989**, *61*, 673–684. (d) Landau, E. M.; Popovitz-Biro, R.; Levanon, M.; Leiserowitz, L.; Lahav, M. *Mol. Cryst. Liq. Cryst.* **1986**, *134*, 323–335. (e) Popovitz-Biro, R.; Jacquemain, D.; Leiserowitz, L.; Lahav, M.; manuscript in preparation.
(4) (a) Grayer Wolf, S.; Leiserowitz, L.; Lahav, M.; Deutsch, M.; Kjaer, K.; Als-Nielsen, J. *Nature* **1987**, *328*, 63–66. (b) Kjaer, K.; Als-Nielsen, J.; Helm, C. A.; Laxhuber, L. A.; Möhwald, H. *Phys. Rev. Lett.* **1987**, *58*, 2224–2227. (c) Dutta, P.; Peng, J. B.; Lin, B.; Ketterson, J. B.; Prakash, M.; Georgopolus, P.; Ehrlich, S. *Phys. Rev. Lett.* **1987**, *58*, 2228–2231. (d) Helm, C. A.; Möhwald, H.; Kjaer, K.; Als-Nielsen, J. *Biophys. J.* **1987**, *52*, 381–390.
(5) Grayer Wolf, S.; Deutsch, M.; Landau, E. M.; Lahay, M.; Leiserowitz, L.; Kjaer, K.; Als-Nielsen, J. *Science* **1988**, *242*, 1286–1290.
(6) (a) Als-Nielsen, J.; Christiensen, F.; Pershan, P. S. *Phys. Rev. Lett.* **1982**, *48*, 1107–1110. (b) Braslau, A.; Deutsch, M.; Pershan, P. S.; Weiss, A. H.; Als-Nielsen, J.; Bohr, J. *Phys. Rev. Lett.* **1985**, *54*, 114–117. (c) Helm, C. A.; Möhwald, H.; Kjaer, K.; Als-Nielsen, J. *Europhys. Lett.* **1987**, *4*, 697–703. (d) Richardson, R. M.; Roser, S. J. *Liq. Cryst.* **1987**, *2*, 797–814. (e) Als-Nielsen, J.; Kjaer, K. In *Phase Transitions in Soft Condensed Matter*, The Proceedings of the Nato Advanced Study Institute; Geilo, Norway, 1989, Plenum Press: New York, 1989.
(7) Grayer Wolf, S.; Landau, E. M.; Lahav, M.; Leiserowitz, L.; Deutsch, M.; Kjaer, K.; Als-Nielsen, J. *Thin Solid Films* **1988**, *159*, 29–41.
(8) Guiner, A. *X-ray Diffraction*; Freeman: San Francisco, 1968; pp 121–125.

3. Theoretical Background

Modeling of the PFA Molecule. In the perfluorinated polymer polytetrafluoroethylene, the perfluorinated chains are arranged in a hexagonal lattice and adopt a helical conformation.[9] It was shown that the helicity is an inherent characteristic of perfluorinated chains.[10] Our model molecule possesses this feature and its perfluorinated segment $CF_3(CF_2)_9$ shows approximately a cylindrical outer surface.[5] The ester group in the lower segment of the chain $(CH_2)_2OCOCH_2$ was assumed to adopt an all-trans conformation; the conformation of the α-amino acid head-group was deduced from energy calculation.[5,11] We note that, in view of the low real-space resolution of the data presented here (due to the short q_z range measured, $q_z \leq 0.67$ Å^{-1}), the z coordinate of the individual atoms are required only to an accuracy of about 0.5 Å.

The atomic positions obtained yield a molecular height of 21.7 Å, consistent with the layer spacing derived from the X-ray powder pattern of crystalline PFA.[5] This model was the starting point for refinement to the data. In the refinements (described in detail below), the ester group of the molecule was compressed by about 35% from the all-trans conformation,[12] the molecular length being finally reduced to a value of 19.6 Å.

Bragg Diffraction from PFA Monolayers. For a 2-D periodic structure of a monolayer lying in the xy plane, Bragg diffraction occurs when $\vec{q}_{xy}$, the component of the scattering vector in the plane of the monolayer, coincides with a reciprocal lattice vector[13] $\vec{G}_{hk}$. Thus, no condition is imposed on the vertical component $\vec{q}_z$ of the scattering vector. Therefore, as opposed to 3-D crystals where Bragg diffraction leads to Laue spots corresponding to hkl reciprocal lattice points, a 2-D crystal scatters in rods (labeled Bragg rods, BR) parallel to the $\vec{q}_z$ vector, passing through each reciprocal lattice point G_{hk} in the monolayer plane. The intensity distribution along these rods is modulated by the molecular structure factor and hence by the electron distribution in the constituent molecules of the crystallites.[14,15]

The BR intensity distribution along q_z, $I_{hk}(q_z)$ is proportional to the structure factor, i.e. the 2-D Fourier transform of the electron density of the 2-D *crystalline* part of the monolayer. The molecular structure factor is calculated from the atomic coordinate model of the molecule described above: Each atom (j), with form factor f_j, is at position $\vec{r}_j + \vec{z}_j$, where $\vec{r}_j = x_j\cdot\vec{a} + y_j\cdot\vec{b}$, $\vec{a}$ and $\vec{b}$ are unit cell axes and $\vec{z}_j = z_j\cdot\vec{z}$, $\vec{z}$ being a unit vector normal to $\vec{a}$ and $\vec{b}$. Thus, the molecular structure factor is

$$F(\vec{G}_{hk};\vec{q}_z) = \sum_j occ_j\cdot f_j\cdot\exp[i(\vec{G}_{hk}\cdot\vec{r}_j + \vec{q}_z\cdot\vec{z}_j)]$$

The atomic occupancies occ_j are equal to a value of 1 for all the atoms in the monolayer molecules. For the ions present in the subphase, occ_j is the number of ion of type j per monolayer molecular site and therefore $occ_j \leq 1$. Since the sample is a 2-D powder,[5] the observed BR intensity at a given $2\theta_0$ position, $I^{obs}(2\theta_0,q_z)$, may contain contributions from several reflections hk

$$I^{obs}(2\theta_0,q_z) = I_0\sum_{hk}\{I_{hk}(q_z) + I_{h\bar{k}}(q_z)\}$$

Here, $I_{hk}(q_z) = |V(x)\cdot F(\vec{G}_{hk};\vec{q}_z)|^2 \exp[-q^2\sigma^2]$. The function $V(x)$ describes the interference between the waves which are diffracted up from the monolayer and those that are diffracted down and subsequently reflected up;[14,15] it is seen as a sharp peak at $q_z \approx 0.01$ Å^{-1}. Explicitly, $V(x) = 2x$ for $0 < x \leq 1$ and $2x/[x + (x^2 - 1)^{1/2}]$ for $x > 1$ where $x = 2q_z/q_c$ and $q_c = (4\pi/\lambda)\sin\alpha_c = 0.021\,764$ Å^{-1}. The Debye–Waller factor $\exp(-q^2\sigma^2)$ accounts for the static and thermal diffuseness of the interfaces. The 2θ integrated intensity of the BR, I, is given by

$$I(q_z) = \int I^{obs}(2\theta,q_z)\, d(2\theta) \approx \text{fwhm}(2\theta)\, I^{obs}(2\theta_0,q_z)$$

where fwhm(2θ) is the full width at half-maximum of the diffraction peak. I_0, in $I^{obs}(2\theta_0,q_z)$, is a scaling factor between the measured and the calculated Bragg rod intensities for a given $2\theta_0$ position of the PSD, such that

$$I_0 \propto (ABCD)L_p\phi\psi^2A_c^{-2}(\text{fwhm}(2\theta))^{-1}$$

ABCD is the area contributing to the scattering and varies as $1/\sin 2\theta$ (Figure 1); $L_p = \cos^2 2\theta/\sin 2\theta$ is the Lorentz polarization factor; ϕ' is that fraction of the area ABCD which is covered by the 2-D crystallites;[16] ψ is the fraction of molecules in the monolayer domains which occupy crystalline lattice sites[16] ($(1 - \psi)$ is the fraction of crystal defect sites). We also define for convenience a scaling factor corrected for A_c^2, fwhm(2θ), ABCD, and L_p

$$I_0' \propto \{I_0A_c^2\text{fwhm}(2\theta)\}/\{(ABCD)L_p\} \propto \phi'\psi^2$$

I_0' is a more useful intensity factor since, by definition, it is constant for the different hk reflections, given the monolayer state. In our analysis, we also use I_0'' which is corrected by the same factors as I_0' and, in addition, by the macroscopic coverage A_c/A

$$I_0'' \propto I_0'A/A_c$$

If the number of molecules in the gas phase is negligible,[16] I_0'' is proportional to ψ and should therefore be nearly a constant for the whole series of BR's.

Specular Reflectivity Calculations. Bragg rod intensity profiles provide 3-D information about the 2-D *crystalline part* of the monolayer. The X-ray reflectivity (XR) profiles, in contrast, are determined by the vertical electron density distribution averaged over both *ordered* and *disordered* parts of the monolayer and include also scattering from the subphase.[6] Further, $\vec{G}_{hk}$ is nonzero for BR, but $\vec{G}_{hk} = \vec{G}_{00} = \vec{0}$ for XR. Thus, XR and BR measure different parts of the monolayer structure factor. The XR intensity distribuiton along q_z is given by[6]

$$R(q_z) = R_f(q_z)\exp(-q_z^2\sigma^2)\{|1 + iq_z(\rho A_c/\psi)^{-1}F(\vec{0};\vec{q}_z)|^2\phi' + (1 - \phi')\}$$

$R_f(q_z)$ is the Fresnel reflectivity calculated for a perfect, sharp interface;[6a,b,e] ρ is the electron density of the subphase; with ψ defined above, A_c/ψ is the mean molecular area in the crystalline domains;[16] σ the roughness parameter and ϕ' is the surface fraction covered by the 2-D crystallites. The second term in the equation describes reflection from patches of uncovered water in between the crystalline domains. Its form assumes that nearly all the molecules are contained in the crystalline domains; otherwise it would be modulated by a factor related to $|1 + iq_z(\rho A_c/\psi)^{-1}$

(9) (a) Bunn, C. W.; Howells, E. R. *Nature* **1954**, *174*, 549–551. (b) Clark, E. S.; Muss, L. T. *Z. Kristallogr.* **1962**, *117*, 119–127.

(10) Dixon, D. A.; van Catledge, F. A.; Smart, B. E., *Abst. PAC Conf. Phys. Org. Chem.* **1988**, *9*, A15.

(11) Berkovitch-Yellin, Z. *J. Am. Chem. Soc.* **1985**, *107*, 8239–8253.

(12) (a) This redution in ester length was required in all fittings to the data. The projected molecular area for PFA is 28.5 Å^2, whereas in usual crystal structures of linear esters such as methyl stearate,[12b] it is about 18.3 Å^2. We therefore envisage that the ester group is folding so as to optimize intra- and intermolecular contacts. (b) MacGillavry, C. H.; Wolthius-Spuy, M. *Acta Crystallogr.* **1970**, *B26*, 645–648.

(13) $\vec{G}_{hk} = 2\pi(h\vec{a}^* + k\vec{b}^*)$ where $\vec{a}^*$ and $\vec{b}^*$ are the reciprocal lattice vectors.

(14) Vineyard, G. *Phys. Rev. B* **1982**, *26*, 4146–4159.

(15) Feldenhans'l, R. *Surf. Sci. Rep.* **1989**, *10*, No. 3, 105.

(16) The monolayer consists of crystalline domains and a coexisting gas phase. The crystalline domains are not all perfect 2-D crystals and this is described by the correction ψ. If A_c is the unit cell area, A_c/ψ is the mean molecular area in the crystalline domains (ψ accounts for point defects and vacancies in the crystal lattice). A and A_{gas} are, respectively, the mean molecular area of the monolayer as a whole, and of the gas phase. We have

$$\left(\frac{A}{(A_c/\psi)}\phi'\right) + \left(\frac{A}{A_{gas}}(1 - \phi')\right) = 1$$

Where the two terms in brackets are respectively the fraction of molecules in the crystalline domains, and in the gas phase. If the number of molecules in the gas phase is neglected (assuming $A_{gas} \gg A_c$), then

$$\frac{A}{(A_c/\psi)}\phi' = 1$$

Table I. Pressure Dependence of the Molecular Arrangement of PFA over Pure Water[a]

curve	π, mN/m	d_{10}, Å	d_{01}, Å	$d_{1\bar{1}}$, Å	a, Å	b, Å	γ, deg	A_c, Å^2	t, deg
a, b, c	uncompressed monolayer	5.30	5.23	5.00	5.92	5.84	116.5	30.9	22
d	4	5.22	5.22	4.99	5.85	5.85	116.9	30.5	20
e	10	5.14	5.14	4.98	5.82	5.82	117.9	29.9	17
f	15	5.07	5.07	4.97	5.79	5.79	118.9	29.4	13
g	20	4.97	4.97	4.97	5.74	5.74	120	28.5	<5
h	28	4.97	4.97	4.97	5.74	5.74	120	28.5	<5

[a] The data presented above refer to the curves displayed in Figure 3. a, b, γ, and A_c are the unit cell parameters and area deduced from the obtained d spacing values, and t is the average molecular tilt angle in the $(1,\bar{1})$ plane.

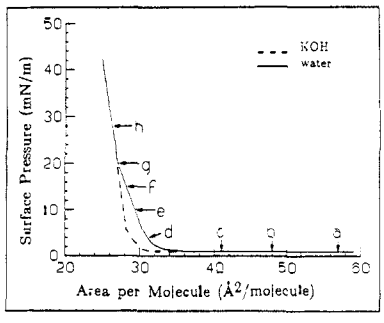

Figure 2. Pressure area ($\pi - A$) diagram of PFA over pure water (full line) and over KOH subphases pH $\geq$ 11.2 (dashed line) at 20 ± 0.1 °C. The arrows indicate the points where the GID measurements were performed over pure water.

$F(\vec{o};\vec{q}_z)|^2$. Only XR data for compressed films are analyzed in this paper, so that ϕ' is close to a value of 1, and hence the equation simplifies to

$$R(q_z) = R_f(q_z)\exp(-q_z^2\sigma^2)|1 + iq_z(\rho A_c/\psi)^{-1}F(\vec{o};\vec{q}_z)|^2$$

The XR data are analyzed by calculating the molecular structure factor from the same atomic coordinate model of the PFA molecule that was used for the BR analysis

$$F(\vec{o};\vec{q}_z) = \sum_j occ_j \cdot f_j \cdot \exp(i\vec{q}_z \cdot \vec{z}_j)$$

The atom occupancies occ_j were defined in the previous paragraph. For the refinement, the model molecule is divided in three segments. These three segments correspond to the α-amino acid $CH(NH_3^+CO_2^-)$, ester $(CH_2)_2OCOCH_2$, and fluorocarbon $CF_3(CF_2)_9$ parts containing 39, 46, and 249 electrons, respectively. The projected lengths of the three segments, the roughness parameter σ, and the molecular area A_c/ψ are obtained from least-square fits to the measured data. For PFA molecules over KOH and CsOH subphases, the atomic coordinate model includes the counterion attached to the α-amino head-group (K^+ or Cs^+). Two additional parameters can be estimated from least-square fits to the data: the distance from the counterion to the head-group box and the percentage of PFA molecules neutralized by a given counterion, which is in fact the occupancy of the counterion. Following earlier practice,[6e] electron density profiles perpendicular to the surface were calculated by using the refined molecular model. Each atom (j), at the final position z_j, is represented by a Gaussian centered on the position z_j. The width of this Gaussian is determined by the smearing parameter σ obtained after refinement and its height is proportional to the product occ_jZ_j, where Z_j is the atomic number of atom j. These Gaussian curves are normalized so that the electron density of the subphase ρ_s is 1.0.

4. Results

4.1. Grazing Incidence X-ray Diffraction from PFA over Water at Different Surface Pressures. The π - A isotherm of PFA over water (Figure 2) shows two changes of slope: one at about 33 Å^2 with zero surface pressure, and another at about 28.5 Å^2, 20 to 25 mN/m. We have monitored the structure of the monolayer by GID both upon monolayer compression (Figure 3a,b) and decompression.[5] For the expanded monolayer with an average molecular area of 1.4–2.0 times the limiting area of 28.5 Å^2 (curves

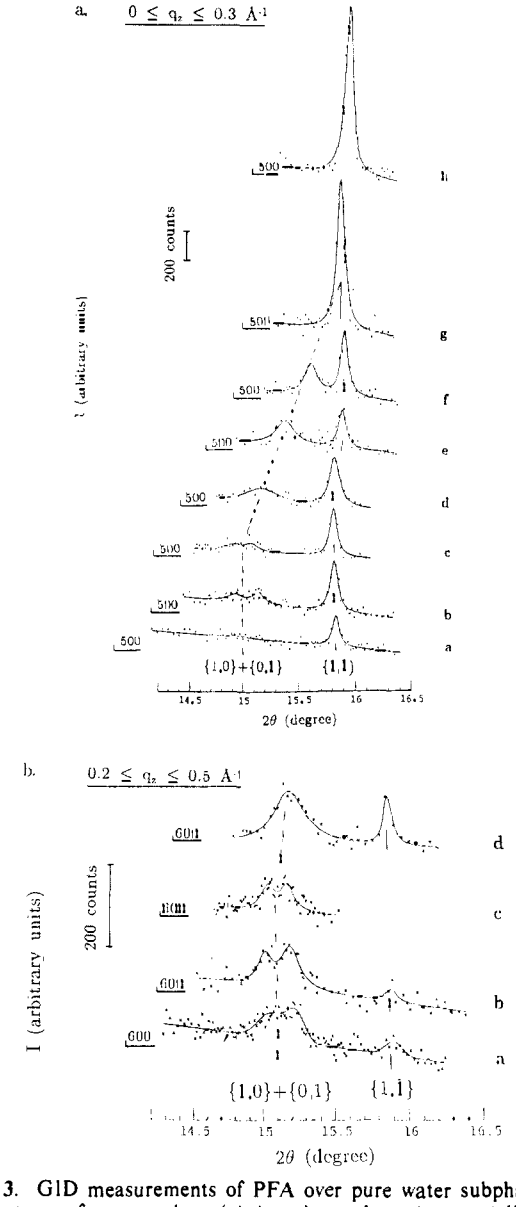

Figure 3. GID measurements of PFA over pure water subphases in various stages of compression. (a) At points a–h on the $\pi - A$ diagram (Figure 2), the acceptance window of the detector corresponds to q_z values between 0 and 0.3 Å^{-1}. (b) At points a–d, on the π - A diagram, the acceptance window of the detector corresponds to q_z values between 0.2 and 0.5 Å^{-1}.

a, b, and c in Figure 3a,b), i.e., for a surface coverage ranging from 50 to 70%, three peaks were observed (a barely resolvable doublet and a singlet). Compression to 4 mN/m results in the two low angle peaks coalescing (curve d in Figure 3a,b). Further compression to above 20 mN/m merges the two remaining peaks to a single intense one (curve g in Figure 3a). Upon decompression below about 25 mN/m the peak splits into two again;[5] however no diffraction peak is observed for the monolayer expanded to point d in Figure 2. Upon decompression[5] over 1 or 2 h, the degree

Table II. Parameters[a,b] for Bragg Rod Fits

subphase	π, mN/m	{h,k}	2θ, deg	fwhm(2θ), deg	L_p·(ABCD)	Ac, Å^2	A_c/A	I_0	I_0'	I_0''
water	28	{1,1̄} + {1,0} + {0,1}	15.96	0.095	12.23	28.5	1.00	0.48	3.04	1.15
water	10	{1,0} + {0,1}	15.43	0.160	13.13	29.9	1.00	0.25	2.24	0.96
		{1,1̄}	15.92	0.095	12.29			0.31	2.84	
water	uncompressed monolayer	{1,0}	14.975	0.165	13.98	30.9	0.54	0.08	0.90	0.68
		{0,1}	15.175	0.140	13.59			0.11	1.08	
		{1,1̄}	15.860	0.090	12.39			0.13	0.92	
KOH, pH = 11.5	uncompressed monolayer	{1,1̄} + {1,0} + {0,1}	15.85	0.109	12.41	28.5	0.57	0.21	1.50	1.00

[a] L_p, ABCD, A_c, fwhm(2θ), I_0, I_0' and I_0'' are defined in the text section 3. A is the mean molecular area of the monolayer;[16] {h,k} are the reflections contributing to the signal. The horizontally collimating solar slit (see Experimental Section) had a resolution of $\Delta(2\theta) = 1.75$ mrad in this case. [b] For the monolayer at 10 mN/m and in the uncompressed state over water, I_0'' is given as an averaged value over the different reflections. I_0'' values are given relative to the value obtained for a reference state: uncompressed PFA over KOH at pH = 11.5 (see Discussion section 5.2).

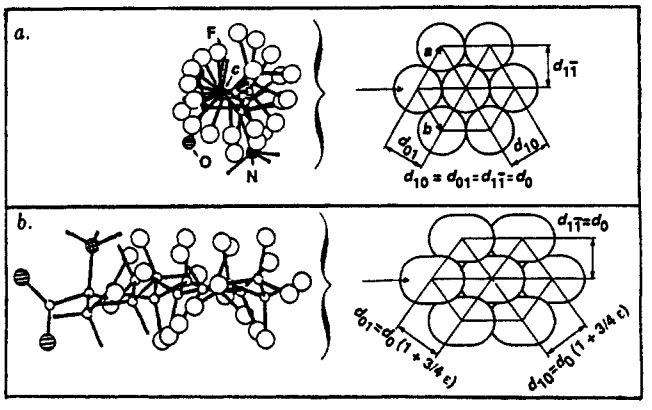

Figure 4. (a) Top view of a model molecule of PFA showing the helical structure of the perfluorinated chain and schematic top view of the high-π structure. (b) Top view of a model molecule of PFA and schematic top view of the low-π structure. The molecules tilt toward nearest neighbors.

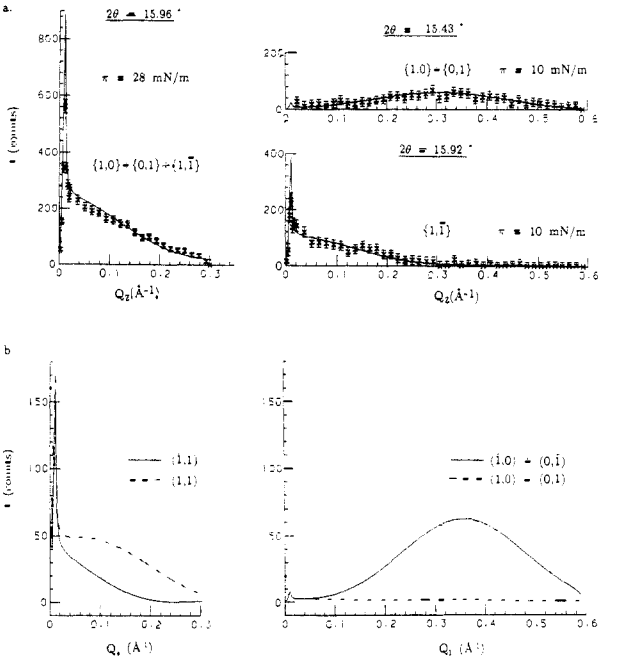

Figure 5. (a) Bragg rod scans of PFA on pure water with calculated fits shown as solid lines (see text for details) for the single GID peak at 28 mN/m (curve h, Figure 3) and for the low angle peak at 10 mN/m (curve e, Figure 3). (b) Calculated Bragg rod profiles for a PFA molecule tilted by 20° in the (1,1̄) plane. The contribution of some combinations of reflection to the signal is shown.

of crystallinity is reduced considerably. This irreversibility observed over water is probably linked to dynamic properties of the system.

4.2. The Pressure Dependence of the Crystalline Structure of PFA Monolayers over Pure Water. At high surface pressure (above 20 mN/m), the single intense peak with a d_0 spacing = 4.97 Å indicates a hexagonal unit cell (Table I) with the three lowest order reflections {1,1̄} = (1,1̄) + (1̄,1), {1,0} = (±1,0), and {0,1} = (0,±1) coinciding in the powder pattern[5] (curves g and h in Figure 3a). The unit cell has axes $a = b = 5.74$ Å, with an area of 28.5 Å^2. At low pressures in the range 1–20 mN/m, the split peak (curves d, e, and f in Figure 3) indicates a distortion of the hexagonal cell which is attributed to the molecules tilting rigidly from the vertical within the (1,1̄) plane[5] (Table I and Figure 4). The low angle peak is identified as the {1,0} + {0,1} reflections and the other as the {1,1̄}.

Further evidence for the tilt, its magnitude and direction is obtained from BR scans.[17] Such scans (Figure 5a) were made upon compression of the PFA monolayers at the high (2θ = 15.92°) and low angle (2θ = 15.43°) GID peaks at 10 mN/m (curve e in Figure 3), and for the single peak position (2θ = 15.96°) at 28 mN/m (curve h in Figure 3). Structural models fitting the BR data were calculated as described in section 3. The BR data at high pressure (Figure 5a and Table II) was fit with vertically aligned model molecules of length 19.6 ± 0.5 Å arranged in a hexagonal unit cell ($a = 5.74$ Å). All six {1,0}, {0,1}, and {1,1̄} reflections contributed to the observed intensity. The fit for the BR data at 10 mN/m (Figure 5a and Table II) was obtained with model molecules tilted at 17° from the vertical in the {1,1̄} plane and arranged in a distorted hexagonal cell ($a = b = 5.82$ Å, $\gamma = 117.9°$). The fit for the low angle BR is obtained as the sum of the {1,0} and {0,1} reflections; the high angle one with the {1,1̄} reflection. The agreement between the observed and calculated BR scans is satisfactory. The corrected scaling factors I_0' (Table II), deduced from the fittings, should be equal for the {1,0} + {0,1} and the {1,1̄} reflections (see section 3). The observed discrepancy can be attributed to uncertainties in the experimental measurements and in our modeling of the system. Figure 5b indicates that for PFA molecules tilted in the (1,1̄) plane, coinciding reflections do not contribute equally to the signal. The calculated BR for the (1,1̄) and (1̄,1) reflections have different profiles, since the PFA molecule does not have mirror symmetry about the (1,1̄) plane. There is practically no intensity arising from the (1,0) + (0,1) reflection, this is the signature of a tilt towards nearest neighbors, i.e. in the (1,1̄) plane.[6e]

A difference is also seen in the X-ray reflectivity (XR) data measured for surface pressures above and below the transition pressure,[18] shown in Figure 6. The molecular model fits (see section 3) are shown by the solid lines. The fit for 28 mN/m is obtained with vertically aligned molecules of molecular length of 19.60 ± 0.50 Å. For 13 mN/m, the reflectivity curve was calculated with molecules tilted by 12° from the vertical in the (1,1̄) plane. Simultaneously, the fitted molecular area increased from 28.9 ± 0.3 to 29.4 ± 0.2 Å^2, a value close to 28.9/cos 12°. These observations indicate that, with reduction of pressure, the molecules

(17) Jacquemain, D.; Grayer Wolf, S.; Leveiller, F.; Lahav, M.; Leiserowitz, L.; Deutsch, M.; Kjaer, K.; Als-Nielsen, J. *Colloque de Physique*, **1989**, *50*, Suppl. No. 10, Colloque C7, 29–36.

(18) The XR profiles shown in Figure 6 are significantly different than profiles presented in previous publications.[5,17] Further, the values of the refined molecular areas are lower than values published previously.[5] The low-pressure data in Figure 6 (13 mN/m) was measured upon decompression as opposed to the other data sets.

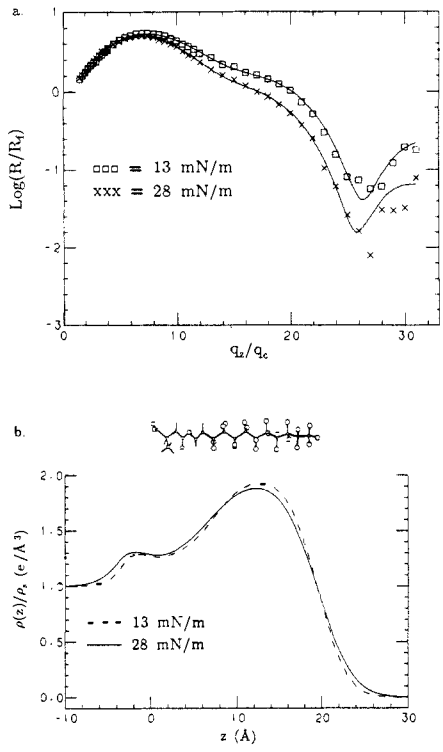

Figure 6. (a) Reflectivity measurements of PFA on pure water. The solid lines are molecular model fits discussed in the text. R/R_f is the measured reflectivity divided by the Fresnel reflectivity calculated for a perfect, sharp interface. (b) Refined relative electron density profiles calculated as described in section 3 (ρ_s is the electron density of the subphase). At the top is shown a side view of the molecule with no tilt, corresponding to the high-pressure model. The profiles obtained at 28 mN/m (full line) and at 13 mN/m (dashed line) are shown in the same frame for comparison.

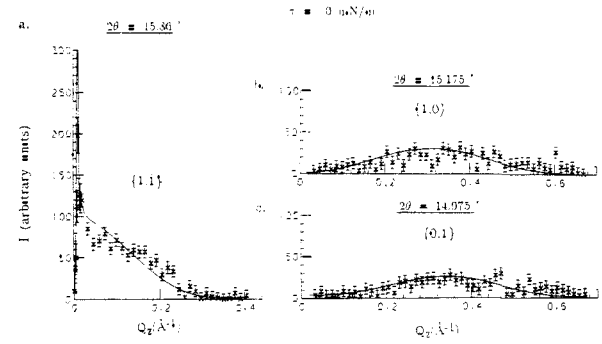

Figure 7. Bragg rod scans of PFA meaured for the first three order GID peaks on curve a in Figure 3. Calculated fits are shown as solid lines: (a) $2\theta = 15.86°$; (b) $2\theta = 15.175°$; (c) $2\theta = 14.975°$.

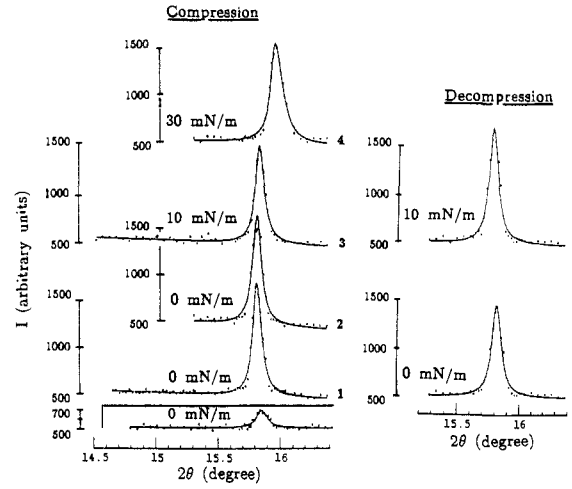

Figure 8. GID measurements of PFA over KOH subphases (pH ≥ 11.2). The acceptance window of the PSD corresponds to q_z values between 0 and 0.26 Å^{-1} for all curves except the bottom spectrum on the left. For the latter, the acceptance window of the PSD corresponds to q_z values between 0.20 and 0.50 Å^{-1}. (1) The molecular area was 50 Å^2, zero surface pressure (uncompressed state). (2) The molecular area was 36 Å^2, zero surface pressure. (3) Surface pressure is 10 mN/m. (4) Surface pressure is 30 mN/m.

tilt almost rigidly and remain close packed. The lattice strain is then $\epsilon = (1/\cos t)-1$, t being the tilt angle.[5,17] Similar results were obtained with monolayers of arachidic acid.[19] The associated splitting of the GID peaks was deduced[5] as $\Delta d = {}^3/_4 d_0 \epsilon$ (Figure 4). For PFA, using $t = 12°$, this gives $\Delta d = 0.0834$ Å in good agreement with the value of 0.090 ± 0.005 Å measured from the 15 mN/m GID data shown in Figure 3 (curve e) where the two peak positions correspond to d spacings of 4.97 and 5.07 Å. Table I displays, as a function of surface pressure, the d spacing values deduced from the peaks positions in Figure 3. The results indicate a continuous reduction of lattice strain ϵ and, in consequence, of the molecular tilt angle upon compression.

4.3. Structure of Self-Aggregated Crystallites of PFA over Various Subphases. Pure Water Subphases. The distinct diffraction peaks observed in the GID results for zero surface pressure (curves a, b, and c in Figure 3) prove the existence of crystalline order even in the so called "gas" or "liquid-expanded" phase. The high-angle peak width[20] is equal to that of the high-pressure peak (curve h in Figure 3) and yields a crystalline coherence length greater than 1500 Å.

Self-aggregated crystallites of PFA did not show any change in their diffraction pattern over a 24-h period, indicating high stability. No significant peak intensity variation was observed on rotation of the trough by 15° which indicates that the samples are two-dimensional powders.

The observation of three peaks (curves a, b, and c in Figure 3) shows that the unit cell of the self-assembled crystallites is no longer hexagonal but oblique ($a = 5.92$, $b = 5.84$ Å, $\gamma = 116.5°$, area = 30.9 Å^2). The d spacing corresponding to the $\{1,\bar{1}\}$ reflection is preserved, indicating a molecular tilt in the $(1,\bar{1})$ plane (Figure 4). The relative change in $|a + b| = 6.19/5.74 = 1.078$, corresponds to an average molecular tilt angle of 22°, on the assumption that the original chain to chain distance of 5.74 Å is preserved at zero pressure. BR scans for the observed reflections on uncompressed PFA (curve a in Figure 3) exhibit significant intensity over background, attesting to the pronounced crystalline character of the samples (Figure 7a,b,c). The fits in the figure are calculated as described in section 3, with model molecules tilted at $t = 22°$ from the vertical and arranged in the oblique cell $a = 5.92$, $b = 5.84$ Å, $\gamma = 116.5°$. The BR profile at $2\theta = 15.860°$ (Figure 7a) is calculated from the structure factor of the two $\{1,\bar{1}\}$ reflections. The structure factor of the two {1,0} reflections contribute to the calculated BR intensity profile at $2\theta = 15.175°$ (Figure 7b). Finally, the fit for the BR measured at $2\theta = 14.975°$ is obtained with contribution of the two {0,1} reflections. The parameters for the fits are tabulated in Table II. The values of the corrected scaling factors I_0', deduced from the fittings (Table II), are equal (within experimental errors), in keeping with a reliable model.

GID measurements of PFA with varying pH demonstrated crystalline self-aggregation for pH values between 4.0 and 11.0 (HCl, NaOH, KOH, or CsOH in the subphase) with coherence lengths exceeding 1500 Å. Detailed measurements for subphase pH's 1.5 and 11.1–11.5 are described below.

Basic Subphases. Over KOH solutions with pH ≥ 11.2, the noncompressed PFA (average molecular area 50 Å^2) yields a single intense GID peak indicating a hexagonal cell ($a = 5.74$ Å, area = 28.5 Å^2) and a coherence length exceeding 1500 Å (curve 1

(19) Kjaer, K.; Als-Nielsen, J.; Helm, C. A.; Tipman-Krayer, P.; Möhwald, H. *J. Phys. Chem.* **1989**, *93*, 3200–3206.

(20) The {1,0} and {0,1} reflections give consistently broader diffraction peaks (Figure 3), yielding lower peak intensities and coherence lengths than the $\{1,\bar{1}\}$ reflection. This may be due to the slight difference between d_{10} and d_{01} values; the two {1,0} and {0,1} reflections never being completely resolved.

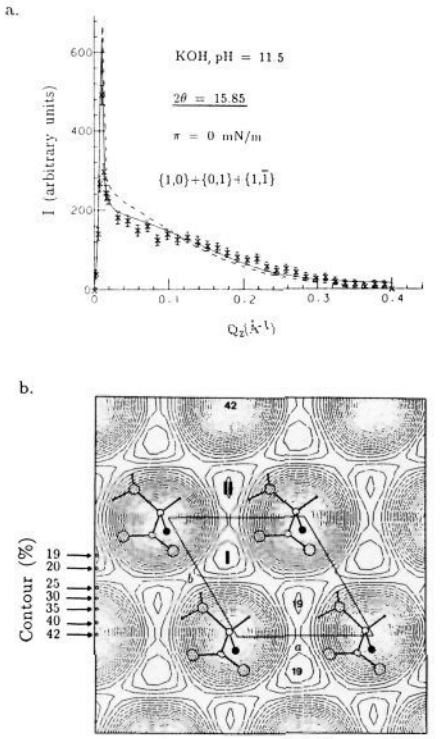

Figure 9. (a) Bragg rod scan of uncompressed PFA over KOH subphase, measured at $2\theta = 15.85°$ (curve 1 in Figure 8). Calculated fit with contribution from the PFA molecules and K^+ ions is shown as a solid line. Calculated fit excluding K^+ ions is shown as a dashed line. (b) R factor[21] contour map (interval 1%) obtained from BR fit as a function of moving the K^+ over the PFA unit cell at a fixed z position. It shows the most probable positions in the (x,y) plane of the K^+ ion. The two sites, with the lowest R factor of 19% (labeled I and II), correspond to where the K^+ ion is expected to occupy. Our model (see discussion, section 5.1) is in favor of a K^+ ion situated at site I. The monolayer unit cell is shown with four α-amino acid head-groups. The carbon atom in black is the first atom of the hydrophobic chain (not shown here for clarity).

in Figure 8). The BR data (Figure 9a) was fitted with a vertically aligned model molecule. The contribution of the six $\{1,\bar{1}\}$, $\{1,0\}$, and $\{0,1\}$ reflections from the PFA molecule cannot account for the observed intensities (dashed line, Figure 9a). We added to the structure factor the contribution from a K^+ ion to fit the observed BR data (full line, Figure 9a). This contribution reduced the R factor[21] of the fit to the observed data by as much as 23% as shown in Figure 9b. The K^+ ion can sit in either of two specific lattice sites corresponding to a minimum R factor of 19% (Figure 9b).

A reduction of the subphase pH from values ≥ 11.2 to a value of 11.1 changes the packing of the PFA self-assembled crystallites. Three GID peaks are observed (curve 1 in Figure 10), a doublet with peak positions of $2\theta = 15.23°$ and $2\theta = 15.68°$ which was resolved by lifting up the PSD ($0.20 \leq q_z \leq 0.50$ Å^{-1}), and a peak at $2\theta = 15.80°$. The doublet is identified as the $\{1,0\}$ and $\{0,1\}$ reflections, the high-angle peak as the $\{1,\bar{1}\}$ reflection. These peaks indicate an oblique unit cell, $a = 5.93$, $b = 5.76$ Å, $\gamma = 118.6°$, area 30.0 Å^2. The relative change in $|a + b|$ from the compressed state is $5.97/5.74 = 1.045$ and corresponds to an average molecular tilt of 18°, smaller than that over water.

Acidic Subphases. HCl subphases (pH = 1.5) also induce changes in the molecular packing of the crystallites. In the noncompressed state, for an average molecular area of 50–41 Å^2, molecules of PFA are arranged in a distorted hexagonal cell ($a = b = 5.92$ Å, $\gamma = 115.6°$, molecular area 31.6 Å^2), as indicated

(21) The R factor is given by

$$R(I(q_z)) = \sum_{q_z}|I_o(q_z) - I_c(q_z)|/\sum_{q_z}I_o(q_z)$$

where $I_o(q_z)$ is the observed intensities and $I_c(q_z)$ is the calculated intensities.

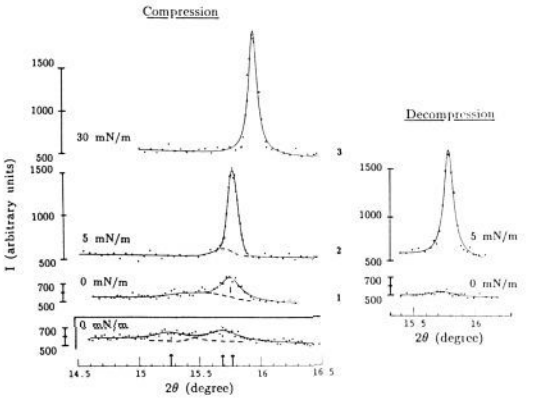

Figure 10. GID measurements of PFA over KOH subphases (pH = 11.1). Very similar results were obtained for CsOH subphases at pH = 11.1. The acceptance window of the PSD in the $\vec{q}_z$ direction was 0–0.26 Å^{-1} except for the bottom spectrum on the left. For the latter the q_z acceptance window was 0.20–0.50 Å^{-1}. (1) The molecular area was 45 Å^2, zero surface pressure. (2) Surface pressure is 5 mN/m. (3) Surface pressure is 30 mN/m.

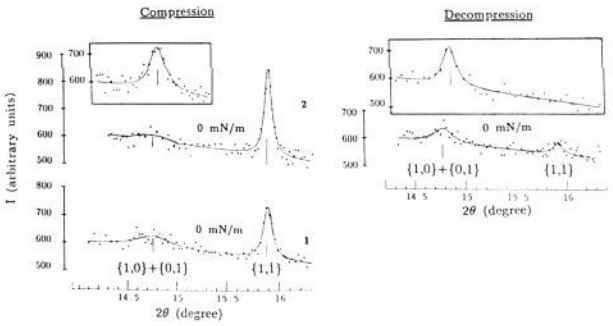

Figure 11. GID measurements of PFA over HCl subphases (pH = 1.5). The acceptance window of the PSD in the $\vec{q}_z$ direction was 0–0.26 Å^{-1} except for the two framed spectra. The latter were measured with a q_z window of 0.20–0.50 Å^{-1}. (1) The molecular area was 50 Å^2, zero surface pressure. (2) The molecular area was 41 Å^2, zero surface pressure.

by the observed doublet (curves 1 and 2 in Figure 11). The intensities of the peaks at $2\theta = 14.75°$ and 15.90° prior to compression are compatible with a molecular tilt in the $(1,\bar{1})$ plane, as over pure water. The change in $|a + b|$ from the compressed state is $6.31/5.74 = 1.099$ which yields an average molecular tilt from the vertical of 25°.

4.4. Monitoring Growth of PFA Crystallites by X-ray GID Measurements. Time-resolved GID measurements of the crystallite growth of PFA over pure water are not feasible as the measuring time is too long compared to the time required for self-aggregation. Preliminary results showed that addition of glycine to the aqueous subphase impedes the growth of the PFA crystallites. We monitored, for the first time, the evolution of the crystallites in real time by GID by using PFA spread over glycine subphases (0.015 M) with an average molecular area of 45 Å^2. Strikingly, 10 min after deposition of the surfactant, no GID signal could be detected (Figure 12a), implying that crystalline order ranged at most over a few tens of angstroms. The integrated peak intensity reaches a plateau about 50 min after deposition (Figure 12b), implying a saturation of the number of ordered molecules; the coherence length takes more time to settle down to a value ≥ 1500 Å (Figure 12b).

4.5. Crystalline Structure of PFA Monolayers at High and Low Pressures over Acidic and Basic Subphases. Upon compression and decompression of the monolayer at a pH ≥ 11.2, the single high-intensity peak is preserved (Figure 8), unlike on pure water. Upon compression to 30 mN/m from the point where the average molecular area is 50 Å^2 (57% coverage), the integrated intensity of the peak does not increase and the peak becomes broader, yielding a coherence length of only about 900 Å. Upon release

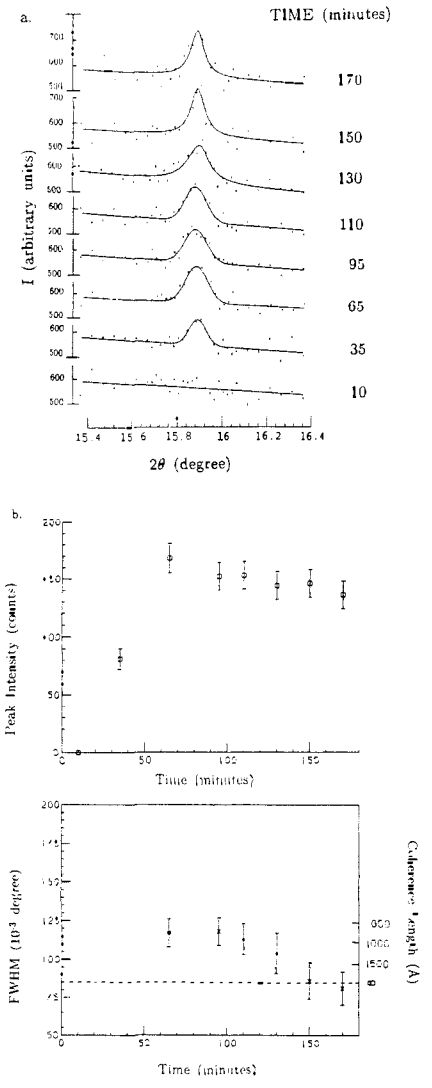

Figure 12. Uncompressed monolayer of PFA over glycine subphases (0.015 M). The molecular area was 45 Å^2: (a) GID measurements as a function of time after spreading (measured $\{1,\bar{1}\}$ reflection); (b) Integrated peak intensity (top) and coherence length (bottom) as a function of time after spreading (due to the low intensity of the peak at 35 min, the coherence length cannot be determined with confidence). The dashed line indicates the resolution limit of the detector.

of pressure, the peak becomes sharp again yielding a coherence length greater than 1500 Å.

For basic subphases at pH = 11.1 (KOH and CsOH), upon compression to intermediate pressures (5–10 mN/m), a high-intensity peak is observed on top of a barely resolvable broad signal (curve 2 in Figure 10). This suggests two different types of domains: one corresponding to the high-intensity peak and so incorporating the overriding number of molecules, which are arranged in a hexagonal cell; the other containing a small fraction of the molecules which are arranged in a somewhat different cell. Further compression leads as always to a single intense GID peak. In contrast to over water subphases,[5] PFA monolayers decompressed to 5 mN/m still display a single intense peak (curve 2 in Figure 10), showing stabilization of the packing. Complete release of pressure, however, results in the disappearance of the GID signal, as over pure water subphases. This suggests that the concentration of bound monovalent cations is not sufficient to maintain the crystalline arrangement in this case.

The XR profiles measured for compressed PFA monolayers over CsOH at pH = 11.1 and KOH at pH = 11.2 subphases confirm the suggested differences in binding (Figure 13a,b). The molecular model fits were calculated as described in section 3. The model PFA molecule is standing vertically, has a length of 19.6 ± 0.5 Å and a molecular area refined to 29.0 ± 0.5 Å.^{2} The refined distance of the Cs^+ and K^+ ions to the plane containing the carboxylate oxygens of the α-amino acid head groups is 1.5 ± 0.5 Å. Simple geometric considerations[22a] tell us that an ionic layer about 3.0 Å thick below the carboxylate oxygens can contain, in addition to the cation, maximally two water molecules per monolayer molecule. When adding to our atomic molecular model two water molecules at the same height as the cation, the atomic occupancies for Cs^+ and for K^+ were refined to 0.35 ± 0.05 and 0.95 ± 0.05, respectively.

Over acidic subphases with pH = 1.5, upon compression to 30 mN/m and decompression to an average molecular area of 41 Å^2, the positions of the two peaks remain the same as prior to compression, but their relative intensities are very different; the $\{1,\bar{1}\}$ reflection gives a very weak, but still observable signal, whereas the intensity of the $\{1,0\} + \{0,1\}$ peak is still preserved (curve 2 in Figure 11). We also note that the coherence lengths are considerably smaller after decompression, indicating a decrease in the degree of crystallinity. The $\{1,\bar{1}\}$ reflection of Figure 11 yields a coherence length of 800 ± 200 Å.

4.6. Probing the Packing of the Polar Head-Groups via Oriented Nucleation of NaCl underneath PFA Monolayers. PFA monolayers promote growth of NaCl at the interface from the {110} and the {111} faces[3c,d] (in contrast to the {100}, which is the naturally occurring and more stable face in water solutions[23]). At neutral pH, the {110} face of NaCl crystals is preferentially attached to PFA monolayers. The {110} face contains alternating rows of Na^+ and Cl^- ions separated by 2.8 Å (Figure 14a). We deduce that at this pH, the head-groups of the monolayer are zwitterionic $^+H_3NCHCO_2^-$, thus forming rows of NH_3^+ and CO_2^- moieties. The distance between these two moieties (2.6 Å) matches fairly well with the separation between point charge rows in the {110} face of NaCl. In contrast, at high basic pH by addition of NaOH (pH > 11.1), PFA induces nucleation of NaCl from the metastable {111} face. All atoms at the surface of a pure {111} layer are of the same kind, either Na^+ or Cl^- (Figure 14b). Thus we deduce that the Na^+ ions bound to the anionic $H_2NCHCO_2^-$ groups of the monolayer expose to the NaCl solution an equipotential atomic layer, suitable for nucleation of NaCl via its {111} face. These results imply that the monolayer molecules in the 2-D crystals are being transformed from a zwitterionic to an anionic charged head-group for basic pH around 11.1. The 3-D epitaxial growth of NaCl from its {110} face in acidic pH can be explained by inclusion of Cl^- ions in between the α-amino acid moieties. This way, rows of positive and negative charges would be created at the surface, which could simulate the repeat motif of the charge distribution in the {110} face. We should stress that, in all three regimes, the point charge distribution of the attached NaCl face is incommensurate with the point-charge distribution offered by the monolayer and the attached counterion. We may interpret the crystallization results in terms of equipotential lines separated by 2.6 Å for the {110} face, or surface for the {111} face, which can concentrate ions with interionic distances comparable to the one observed on the crystal faces.

5. Discussion

The detection of self-assembled crystalline clusters for the noncompressed PFA monolayer at the interface is a clear indication that the traditional monolayer phase assignment[24] (i.e.,

(22) (a) The water molecules are considered as spheres of volume 30 Å^3 (volume of a water molecule in bulk liquid water). The distances between K^+ ions, Cs^+ ions, and water molecules in known crystal structures of hydrate of carboxylic acid salts of these cations[22b,c] are, respectively, 2.85 ± 0.05 and 3.35 ± 0.05 Å. The PFA unit cell surface A_c = 28.5 Å^2 can accommodate 1.5 Å below the carboxylate oxygens, one cation and two water molecules in a layer of thickness 3 Å. (b) Geise, H. J.; van Loock, J. F. J.; Lenotra, A. T. H. *Acta Crystallogr.* **1983**, *C39*, 69–70. (c) Gupta, M. P.; Mahata, A. P. *Cryst. Struct. Commun.* **1976**, *5*, 557–560.

(23) The relative stability of the faces is {100} > {110} > {111}. This is readily understood in terms of electrostatic interactions between ions in the faces. In the {100} face each ion is surrounded by four ions of opposite charge at 2.8 Å, in the {110} face by two ions of opposite charge at 2.8 Å, whereas in the {111} face all ions are of like charge.

(24) Gaines, G. L., Jr. *Insoluble Monolayers at Liquid-Gas Interfaces*; Wiley: New York, 1966

Table III. pH Dependence of the Molecular Arrangement of the PFA Crystallites[a]

subphase	pH	a, Å	b, Å	γ, deg	A_c, Å^2	t, deg	L, Å
			Uncompressed Monolayer				
KOH	11.5	5.74	5.74	120	28.5	<5	≥1500
KOH	11.1	5.93	5.76	118.6	30.0	18	≥1500
H_2O	5.8	5.92	5.84	116.5	30.9	22	≥1500
HCl	1.5	5.92	5.92	115.6	31.6	25	≥1500
			Compressed Monolayer				
KOH	11.5	5.74	5.74	120	28.5	<5	900
KOH	11.1	5.74	5.74	120	28.5	<5	≥1500
H_2O	5.8	5.74	5.74	120	28.5	<5	≥1500

[a] a, b, γ, and A_c are the unit cell parameters and area, t is the average molecular tilt angle, and L is the coherence length for the $\{1,\bar{1}\}$ reflection defined in section 2.

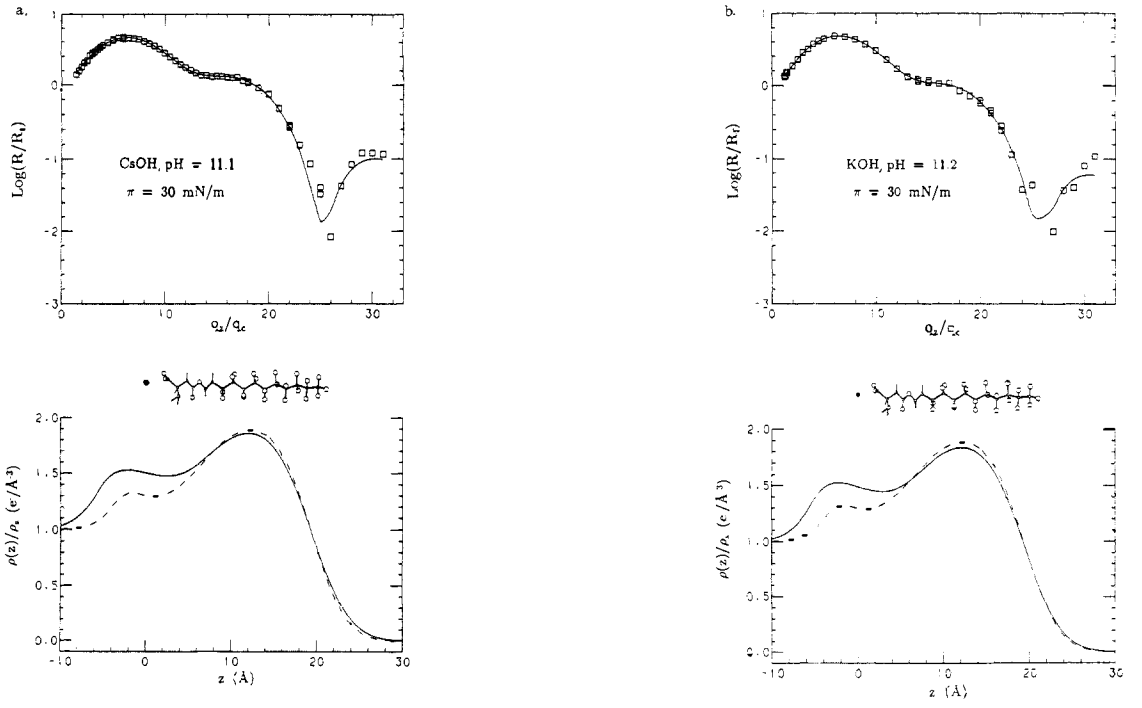

Figure 13. Top. Reflectivity measurements of PFA on basic subphases. The solid lines are molecular model fits discussed in the text. R/R_f is the measured reflectivity divided by the Fresnel reflectivity calculated for a perfect, sharp interface. Bottom. The refined relative electron density profiles (bottom) calculated as described in section 3 (ρ_s is the subphase electron density). At the top of each profile is shown a side view of the model molecule with the attached counterion (Cs^+ or K^+, filled atom). The water molecules contained in the ionic layer are not shown. The electron density profile (dashed line) obtained at high surface pressure over water (Figure 6) is shown as a reference. (a) Set is for CsOH pH = 11.1. (b) Set is for KOH pH = 11.2.

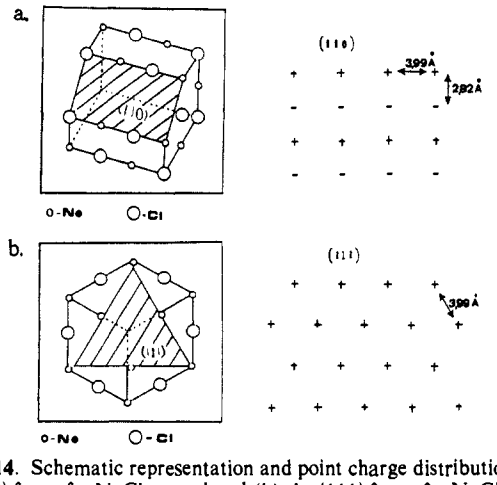

Figure 14. Schematic representation and point charge distribution of (a) the {110} face of a NaCl crystal and (b) the {111} face of a NaCl crystal.

"gas", "liquid expanded", "liquid condensed", and "solid"), loosely based upon macroscopic measurements, is misleading in some systems. For water subphases at various pH's, the self-aggregation of the crystallites is a very fast process since a few minutes after deposition, crystalline coherence lengths ≥ 1500 Å are measured (Table III). On the basis of the results presented above, we now discuss the possible driving forces for the self-aggregation process.

5.1. Modeling of the Head-Group Arrangement in the Crystallites at Various pH's. Strong support for the major role played by the α-amino acid head groups in the PFA self-aggregation is obtained from the experimental results. For instance, significant differences in structure and growth rate of the PFA crystallites are induced by the presence of ions or solute molecules in the liquid layer directly below the hydrophilic head groups. These changes are most probably due to differences in head-group packing and ionization state. Indeed, the fluorocarbon chains are confined, due to intramolecular steric factors, to a stiff helical conformation.[5] Chain–chain interactions were shown to be weaker for surfactant perfluorinated molecules than for aliphatic hydrocarbon molecules.[25,26] In addition, we did not obtain any GID peak from calcium or cesium perfluorodecanoate surfactants at room temperature, where the head-group is a simple carboxylate instead of the α-amino acid moiety. Hence, the intermolecular interaction between the perfluorinated chains do not play a dominating role for self-aggregation.

(25) Mukerjee, P.; Korematsu, K.; Okawauchi, M.; Sugihara, G. *J. Phys. Chem.* **1985**, *89*, 5308–5312.
(26) Arrington, J. R.; Patterson, G. D. *J. Phys. Chem.* **1953**, *57*, 247–250.

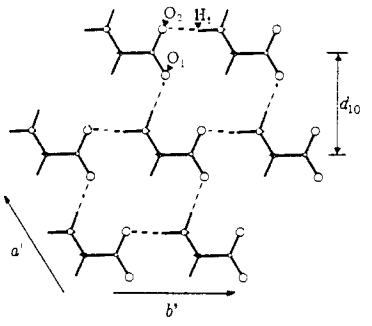

Figure 15. *a'b'* layer[41] of a glycine crystal viewed along the *c'* axis. The dashed lines represent hydrogen bonds. The interlayer spacing in the *a'b'* plane is d_{10}. H_1, O_1, and O_2 are atoms mentioned in the text.

Earlier structural studies on PL[4a] and PFA[5] monolayers also proved the importance of the hydrogen bonds at the α-amino acid head groups to understand the molecular packing of these crystalline monolayers. These hydrogen bonds are the main connections between the CO_2^- and NH_3^+ moieties at the head-group of two neighboring molecules. The crystal packing deduced from the measured GID results (Table III) did not give any direct information concerning the geometry of the head-groups in the hydrophilic layer. Nevertheless, it is possible to deduce the overall packing characteristics of the head-group in its zwitterionic state ($^+H_3NCHCO_2^-$) over pure water and ionized states at high ($H_2NCHCO_2^-$, K^+) and low pH ($^+H_3NCHCO_2H$, Cl^-), which we discuss in turn.

The cell axes of PFA (Table III) derived from the diffraction data in the uncompressed and compressed states over pure water are, respectively, $a = 5.92$, $b = 5.84$ Å, $\gamma = 116.5°$ and $a = b = 5.74$ Å, $\gamma = 120°$ where the "natural" cell for $^+H_3NCHCO_2^-$ moiety is $a' = 5.10$, $b' = 5.46$ Å, $\gamma' = 112°$ as in the crystal structure of α-glycine[27] (Figure 15). In the hydrogen-bonding motif of the latter the two N-H···O distances are 2.95 Å, which implies that the molecule of PFA cannot be interconnected as α-glycine by N-H···O bonds.

Nevertheless, we may construct the hydrogen-bonding motif of the α-amino acid head-groups of uncompressed PFA as follows: A chain connecting the head groups by N-H···O (carboxylate) bonds may be formed along the *b* axis of 5.84 Å by linking the $N-H_1$ bond, not to oxygen O_2 as in α-glycine (Figure 15), but to oxygen O_1 as shown in Figure 17a,b (dotted lines). This chain motif is found in the crystal structures of L-alanine,[28] D,L-alanine,[29] and neopentylglycine[30] (Figure 16), with axial lengths of 5.78, 5.82, and 5.84 Å, respectively. Thus the chain is preferentially formed in PFA along *b*, rather than *a* which is 0.08 Å longer; it cannot be formed along the $a + b$ axis of 6.19 Å, which is too long (Figure 17a). But this chain motif precludes the carboxylate oxygen O_2 from participating in a second N-H···O bond; besides, the adjacent chains along the *a* axis are too far separated to be interlinked by N-H···O bonds (the layer spacing d_{10} for α-glycine is 4.73 Å, whereas it is 5.30 Å for the uncompressed monolayer over water), other than by participation of two water molecules per α-amino acid moiety, as in the crystal structure of neopentylglycine (Figure 16). In this crystal structure the side chain is too bulky to permit the α-amino acid moieties to form a hydrogen-bonded layer as in α-glycine, so the molecules form a sublattice[30] $a' = 6.55$, $b' = 5.84$ Å, $\gamma' = 126°$, area $a'b' \sin \gamma' = 30.7$ Å^2 (Figure 16a). This molecular area is very close to that of uncompressed PFA (30.9 Å^2). Further, the neopentylglycine interlayer d_{10} spacing containing a ribbon of water molecules is $d_{10} = 6.55 \sin 126° = 5.30$ Å (Figure 16a). This interlayer spacing is the same as the one deduced from GID measurements for the uncompressed PFA over water: $d_{10} = 5.92 \sin 116.5° = 5.30$ Å

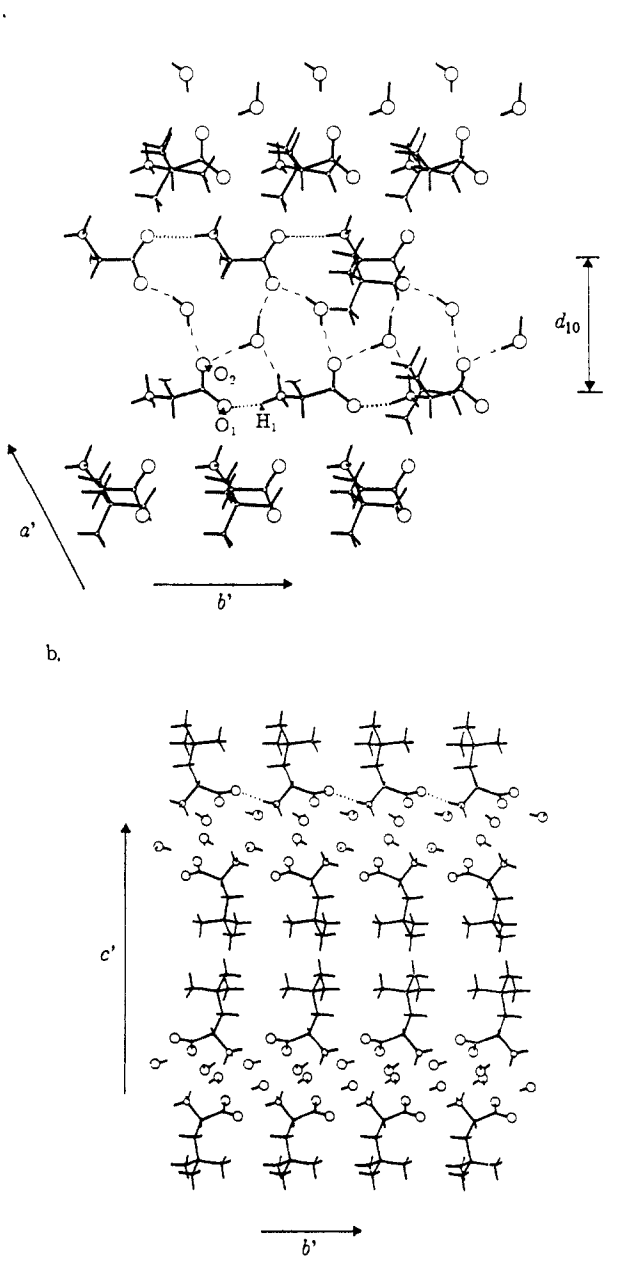

Figure 16. (a) *a'b'* layer of neopentylglycine[41] showing the ribbons of water molecules bridging the strands of α-amino acid molecules. The hydrogen-bond motif is shown for a bilayer (dashed and dotted lines). d_{10} is the interlayer spacing including one ribbon of water molecules. H_1, O_1, and O_2 are the atoms mentioned in the text. For clarity, molecules in one unit cell are shown without their side chains. (b) View along *a'* showing the layerlike packing of a neopentylglycine crystal. A bilayer of water molecules interlink the neopentylglycine layers.

(Figure 17a). The proposed motif of hydrogen bond is then similar to that of neopentylglycine and is shown in Figure 17a. Parallel strands of PFA molecules are interlinked by ribbons of water molecules. As deduced from our data, the chain tilt is along the $a + b$ axis of 6.19 Å (Figure 17b).

At pH ≥ 11.2, the noncompressed PFA molecules are aligned vertically in a hexagonal cell with a molecular area of 28.5 Å^2, as low as in the fully compressed crystalline state (Table III). The X-ray reflectivity measurements over KOH as well as oriented crystallization of NaCl under PFA point to the α-amino acid head-groups being in the anionic state ($NH_2CHCO_2^-$) at pH ≥ 11.2. The hexagonal cell in the uncompressed state may be explained as follows: the most reasonable position for the unicharged cation (Na^+, K^+, Cs^+) is between the carboxylate oxygen atoms O_1 and O_2 of neighboring molecules (Figure 18a), as in other soap structures,[31] since the net charge on each oxygen ion is about 0.5 e. Atoms O_1 and O_2 are separated by about 3.5 Å

(27) Legros, J. P.; Kvick, A. *Acta Crystallogr.* **1980**, *B36*, 3052-3059.
(28) Lehmann, M. S.; Koetzle, T. F.; Hamilton, W. C. *J. Am. Chem. Soc.* **1972**, *94*, 2657-2660.
(29) Donohue, J. *J. Am. Chem. Soc.* **1950**, *72*, 949-953.
(30) Weissbuch, I.; Frolow, F.; Addadi, L.; Lahav, M.; Leiserowitz, L. *J. Am. Chem. Soc.* preceding paper in this issue.

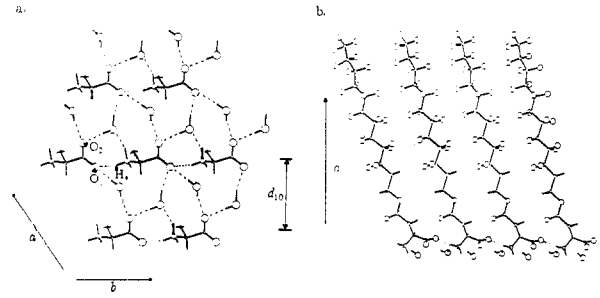

Figure 17. Model arrangement of the PFA molecules in the self-assembled crystallites over pure water. (a) View along c shows the arrangement of the α-amino acid head-groups of the monolayer. The hydrogen bonds are shown as dotted and dashed lines. d_{10} is the interlayer spacing in the ab plane. The atoms H_1, O_1, and O_2 are mentioned in the text. (b) View is along a of the PFA molecules and the attached layer of water molecules, showing in projection the tilt in the $(1,\bar{1})$ plane. The hydrogen bonds between the PFA molecules are shown.

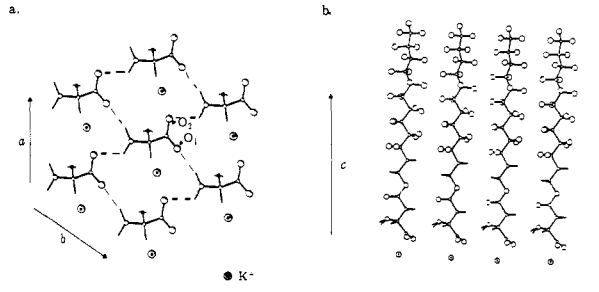

Figure 18. Model arrangement of the PFA molecules in the self-assembled crystallites at high pH (pH $\geq$ 11.2). The water molecules contained in the potassium ionic layer are not shown. (a) View along c shows the hexagonal cell of the monolayer and the attached counterions. Only the α-amino acid head group is shown for clarity. The hydrogen bonds are indicated by dashed lines. (b) View is along a of the PFA molecules and the attached layer of monovalent cations Na^+ or K^+.

and the oxygen–potassium distance in known crystal structures of soap[31] is 2.75 ± 0.05 Å. Therefore, the distance perpendicular to the water surface between K^+ and the plane containing the carboxylate oxygen atoms should be approximately 1.5 Å, in agreement with the XR analysis. Thus the structure is composed of an upper layer of anions and a lower layer of cations, which are binding neighboring PFA molecules. The layer of cations is in the lowest energy state when all nearest neighbor cations are equidistant, leading in this case to a hexagonal cell commensurate with the monolayer cell (Figure 18a). The model arrangement specifying the position of the K^+ is consistent with the BR calculation (Figure 9) according to which the K^+ ion would occupy the position corresponding to either site I or II (Figure 9b). The proposed model corresponds to a K^+ ion at site I. This result validates our model which indicates the existence of an ordered K^+ cationic layer, responsible for the high crystallinity observed in this case. The X-ray reflectivity measurement over KOH subphases at pH = 11.2 shows that two water molecules interleaves in this layer, otherwise its density would be too low. A hexagonal net comprising one K^+ and two water molecules per unit cell suggests that the K^+ ions are 6-fold coordinated by water within the layer. The region around site II in Figure 9b may corresponds to the position of two ordered water molecules which contribute to the scattering: BR fits with a water molecule at site II and a K^+ ion at site I yield a minimum R factor of 14%.

For HCl subphases with pH = 1.5, we can assume that the α-amino acid head-groups are cationic, bearing NH_3^+ charged moieties. This unit charge is probably distributed equally among the three hydrogen atoms and the amino groups are so arranged that there is no short intermolecular distance between neighboring amino hydrogen atoms, unlike between the carboxylate oxygen atoms at high pH (about 3.5 Å). This implies that the Cl^- ions

(31) Dumbleton, J. H.; Lomer, T. R. *Acta Crystallogr.* **1965**, *19*, 301–307.

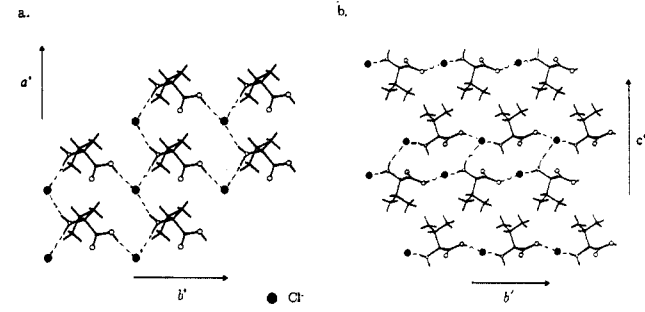

Figure 19. (a) $a'b'$ layer of valine hydrochloride crystal.[41] The dashed lines represent hydrogen bonding. (b) View along a' showing the layerlike packing of a valine hydrochloride crystal. The Cl^- ions are intercalated between valine molecules in planes parallel to $a'b'$ planes. The dashed lines are hydrogen bonds.

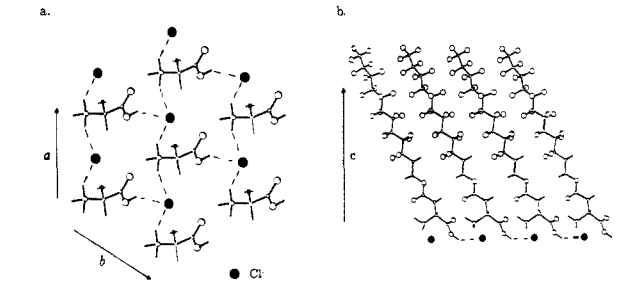

Figure 20. Model arrangement of the PFA molecules in the self-assembled crystallites at low pH (pH = 1.5). (a) View along c shows the distorted hexagonal cell of the monolayer and the attached Cl^- ion. Only the α-amino acid head-group is shown for clarity. The dashed lines indicate hydrogen bonding. (b) View is along a of the PFA molecules and the attached layer of Cl^- ions, showing in projection the tilt in the $(1,\bar{1})$ plane.

can more easily intercalate between the amino groups, which would result in an increase of the unit cell area in the uncompressed state, as is observed (31.6 $Å^2$ instead of 28.5 $Å^2$ at high pH (Table III)). Similar motifs are observed in 3-D crystals of hydrochloride derivatives of α-amino acids such as glycine[32] or valine[33] which possess a layerlike packing (Figure 19b). In each layer of these crystals the cationic α-amino acid molecules are related by translation and are linked by intercalating Cl^- ions, forming hydrogen-bond nets with a repeat molecular area of 36–37 $Å^2$ (Figure 19a). Since the repeat area in the PFA monolayer is only 31.6 $Å^2$, this implies that the Cl^- ions cannot intercalate completely in the monolayer plane but lie about 1 Å below it, linking two NH_3^+ moieties and one CO_2H (Figure 20). Remarkably, the induced crystallization of NaCl underneath PFA monolayers is sensitive enough to allow for the detection of these structural changes on a molecular level. The crystallization from the {110} face in acidic pH could be explained by the Cl^- intercalation at the monolayer head groups.

5.2. Dynamics of Formation and Structural Changes upon Compression of the PFA Crystallites. As mentioned earlier, the rate of growth of PFA crystallites over pure water is too fast to monitor. We could slow down the process by using solute molecules such as glycine which interact with the PFA head-group. Glycine inhibits the growth, probably retarding the approach between the PFA molecules.

The results for the noncompressed monolayers suggest fast formation of large randomly oriented aggregates at different locations on the surace; when mature, these crystallites may be surrounded by water patches nearly free of isolated PFA molecules. Thus, the onset of surface pressure at 32 $Å^2$ in Figure 2 corresponds to the PFA crystallites coming into contact. Over KOH solutions at pH $\geq$ 11.2, the π – A diagram of PFA (Figure 2,

(32) Di Blasio, B.; Pavone, V.; Pedone, C. *Cryst. Struct. Chem.* **1977**, *6*, 745–748.

(33) Koetzle, L.; Golic, L.; Lehmann, M. S.; Verbist, J. J.; Hamilton, W. C. *J. Chem. Phys.* **1974**, *60*, 4690–4694.

dashed line) does not show any change of slope at intermediate pressures. This is consistent with the fact that the surfactant crystal packing does not change upon bringing the crystallites together, since the ordered molecules in the uncompressed state are already vertically aligned with a molecular area as low as 28.5 Å^2 (Table III). On the other hand, both over pure water and at low pH (pH = 1.5), the molecules in the ordered state are tilted from the vertical at about 23° with an area of 30.9 and 31.6 Å^2, respectively (Table III). Thus, upon contact, these PFA molecules will begin to straighten up when the tilted peripheral molecules of neighboring differently oriented crystallites come into contact; the molecular area in the crystalline state reducing eventually to 28.5 Å^2 under full compression.

Several questions relating to change in coherence length and the intensity of the diffraction peaks after compression and decompression at high, neutral, and low pH have to be addressed.

Over a KOH solution at pH ≥ 11.2, compression from 57% to total molecular coverage induced a reduction in coherence length from ≥1500 Å to 900 Å and no increase in the integrated intensity of the diffraction peak. This result suggests *almost total crystallinity in the initial uncompressed state.* When the randomly oriented crystallites come into contact upon compression, the lateral pressures introduce defects into them, reducing the range of perfect crystalline order. Moreover, the number of ordered molecules contributing to the integrated intensity remains almost constant despite the increase of approximately 40% of illuminated molecules, suggesting a distortion of the crystalline order sufficient to offset the contribution to the integrated intensity. We therefore propose that a distortion occurs at the periphery of the crystallites since they have to readjust their shapes to accommodate all the molecules in the fully compressed state. We envisage that these peripheral distortions may propagate to the bulk of the crystallites, thus accounting for the observed reduction in crystallinity on full compression. Further, these distortions may be due to strong electrostatic interperipheral forces coming into play between the anion–cation bilayers of two neighboring crystallites. On release of pressure the original coherence length at the resolution limit of 1500 Å is regained.

Bragg rod analysis, through corrected scaling factor comparison ($1_0''$, Table II), provides us with estimate of the degree of crystallinity of the system at different surface pressures over water and for the uncompressed monolayer over KOH at a pH ≥ 11.2 (Table II). Assuming that in the uncompressed state over KOH all the molecules occupy ordered sites in crystalline domains (i.e. $\psi = 1$, ψ was defined in section 3); it follows that[16] $\phi' = A_c/A = 28.5/50 = 0.57$ which corresponds to the macroscopic coverage of the monolayer. The assumption of total crystallinity is reasonable in view of the GID results described previously. Taking this crystalline state as a reference system, the corrected scaling factor obtained for PFA over pure water at high pressure (Table II) also yields a total crystallinity ($\psi \approx 1$), for a chosen macroscopic coverage[16] $\phi' = A_c/A = 28.5/28.5 = 1$. This result is an indication that, under such pH and surface pressure conditions, PFA molecules are in crystalline domains that cover the whole surface, and the density of point defects in the crystallites is very low, as expected from an ideal compressed phase. It also proves indirectly that the deduction of high crystallinity in the uncompressed state over KOH is probably correct. At 10 mN/m, the crystallinity is comparable to our reference state, PFA uncompressed over KOH (Table II). In the uncompressed state over water, the corrected scaling factor indicates a significantly lower degree of crystallinity of the system. This reduction may have two coupled origins: a higher density of point defect in the crystallites,[16] or a higher fraction of molecules in the gaseous phase[16] than over KOH subphases at pH ≥ 11.2. However, the ratio between the corrected scaling factors is about 70%, indicating still a high degree of crystallinity in the uncompressed PFA over water.

The lower molecular area at high pH rather than over pure water (28.5 vs 30.9 Å^2, respectively), indicates weaker electrostatic interactions between PFA molecules over pure water in the uncompressed state rather than at high pH. The net charges on the zwitterionic carboxylate and amino groups of crystalline α-glycine[11] and L-alanine[34] were derived from electron density deformation distributions using low-temperature X-ray diffraction data. The net charges are approximately 0.4 and −0.4 electron units against the unit charge in the cation–anion system, and so the neighboring misoriented crystallites may be more easily forced to readjust their shapes without an observed reduction in coherence length below the resolution limit. That a residual distortion is introduced on compression is apparent from the disappearance of the diffraction peak upon total decompression.

The behavior of the crystallites at low pH appears to be unusual. Prior to compression the GID results indicate crystallites with a coherence length ≥ 1500 Å in which the molecules are tilted in the $(1,\bar{1})$ plane and are in a distorted hexagonal net (Figure 20). After decompression the GID peak at the low 2θ position of 14.7° maintains its original intensity, but the 2θ peak at 15.9° almost disappears and yields a coherence length of 800 ± 200 Å (due to the low intensity of the peak, the coherence length cannot be determined with confidence). We suggest that this is due to the molecules not tilting exactly in the $(1,\bar{1})$ plane but sufficiently randomly about it as to reduce considerably the coherence length and the intensity corresponding to the $\{1,\bar{1}\}$ reflection ($2\theta = 15.9°$).

We conclude this section by comparing our observations with studies performed on hydrocarbon derivatives both as monolayers over water and on solid supports. X-ray and neutron reflectivity measurements on spread films of docosanoic acid on aqueous subphases containing cadmium ions at different pH's showed similar features.[35] It was concluded that the cadmium ions are bound tightly to the acid head group for pH greater than 5. Moreover, upon decompression to twice the "close-packed" area, it was deduced that the film breaks up into islands of close-packed molecules still perpendicular to the surface; the molecules only tilt if the pH is low enough to displace the cadmium from the acid head-groups. We have made a direct observation of crystalline islands by GID with a different system: arachidic acid monolayers spread over 0.5 M $CuSO_4$ subphases maintained their crystallinity after decompression to twice the "close-packed" area. Transmission electron microscopic studies of deposited uncompressed monolayers of fatty acids also suggested self-aggregation prior to deposition at temperatures lower than the fatty acid melting point.[36] Near-edge X-ray absorption fine structure studies of deposited arachidate salts on Si(111) showed that the cadmium salt is vertically bonded to the surface, whereas the calcium salt is tilted by about 35° from the vertical to the surface.[37] The proposed explanation is that differences in counterion binding to the acid head groups over the aqueous subphase modify the head-groups interactions, thus stabilizing during deposition a perpendicular or a tilted phase. A further example where the head-groups spacing imposes distinct values for the alkyl chain tilt is given by the alkanethiols adsorbed from solution onto metal surfaces.[38,39]

6. Summary and Conclusion

Self-assembled crystalline domains have been detected and their growth monitored by direct methods. Their crystalline structure was studied in detail. The dominant role of the α-amino acid head-groups in the self-aggregation process was demonstrated. Strong indications for organized layers of Cl^- ions, water molecules, and K^+ ions plus water molecules underneath the monolayer head-groups were obtained at low, neutral, and high pH. The formed bilayers (head-group layer and ionic or water layer) were shown to determine the molecular packing and orientation in the

(34) Eisenstein, M., Private communication after Destro, R.; Bianchi, R.; Morosi, G. *J. Phys. Chem.* **1989**, *93*, 4447–4457.
(35) (a) Grundy, M. J.; Richardson, R. M.; Roser, S. J.; Penfold, J.; Ward, R. C. *Thin Solid Films* **1988**, *159*, 43–52. (b) Richardson, R. M.; Roser, S. J. *Liq. Cryst.* **1987**, *2*, 797–814.
(36) Kajiyama, T.; Tanimoto, Y.; Ucchida, M.; Oishi, Y.; Takei, R. *Chem. Lett.* **1989**, 189–192.
(37) Rabe, J. P.; Swalen, J. D.; Outka, D. A.; Stöhr, J. *Thin Solid Films* **1988**, *159*, 275–283.
(38) Strong, L.; Whitesides, G. M. *Langmuir* **1988**, *4*, 546–558.
(39) Ulman, A.; Eilers, J. E.; Tillman, N. *Langmuir* **1989**, *5*, 1147–1152 and references therein.

crystallites. We could obtain an estimate of the degree of crystallinity of the monolayers at different pH's and at a different state of compression. It was concluded that the bilayer formed at high basic pH (pH ≥ 11.2) is the most stable one; the K^+ ions are arranged in a hexagonal cell commensurate with the monolayer cell. The crystalline order in uncompressed PFA monolayers is greatly enhanced in this case. Very recently, we observed similar results with a different system: uncompressed arachidic acid monolayers spread over $CdCl_2$ subphases at 5 °C self-assembled into large crystalline clusters, whereas in the uncompressed state, over pure water, the crystalline order was very low.[40] The X-ray diffraction data also gave an indication of an ordered cadmium ion layer beneath the monolayer.

The obtained structures for the crystallites are in agreement with expectations from NaCl epitaxial crystal nucleation. This confirmation implies that epitaxial crystallization can be a sensitive method for the detection of structured aggregates, as was proposed from studies on short-chain hydrophobic α-amino acids,[30] systems which are not yet amenable to GID measurements.

The results presented in this study open new possibilities for studying nucleation and growth of self-assembling crystals of model systems on a molecular level in two dimensions. The aim would be to monitor the growth of the crystallites from their inception to their mature form, gleaning information on the size and structure of their nuclei.

Acknowledgment. We are grateful to Isabella Weissbuch for assistance, together with Ronit Popovitz-Biro for valuable discussions, and Edna Shavit for synthesizing and purifying the compounds. We thank Ada Yonath at the Max Planck Unit for Structural Molecular Biology for use of laboratory facilities. We acknowledge financial support from U.S./Israel Binational Science Foundation, Jerusalem, the Petroleum Fund administered by the American Chemical Society, the fund for Basic Research of the Israel Academy of Sciences and Humanities, the Minerva Foundation and the Danish Foundation for Natural Sciences, and beam time at the HASYLAB, DESY, Hamburg, FRG.

Supplementary Material Available: Table of PFA atomic fractional coordinates and a structure for PFA (2 pages). Ordering information is given on any current masthead page.

(40) Leveiller, F.; Jacquemain, D.; Lahav, M.; Leiserowitz, L.; Deutsch, M.; Kjaer, K.; Als-Nielsen, J. manuscript in preparation.

(41) The cell axes of various crystal structures were relabeled a', b', and γ' to be consistent with the a, b, γ system of the monolayer.

3-Ureidoacrylonitriles: Novel Products from the Photoisomerization of Cytosine, 5-Methylcytosine, and Related Compounds

Anthony A. Shaw and Martin D. Shetlar*

Contribution from the School of Pharmacy, Department of Pharmaceutical Chemistry, University of California, San Francisco, California 94143. *Received March 1, 1990*

Abstract: During studies of the effects of far-ultraviolet light on DNA and its components, we have discovered that cytosine and 5-methylcytosine, as well as their nucleosides and *N*1-methyl derivatives, undergo photoisomerization reactions to yield the corresponding *cis*- and *trans*-3-ureidoacrylonitriles. For example, *N*1-methylcytosine reacts to give *cis*- and *trans*-3-[*N*3-methylureido]acrylonitrile. These products have been characterized through use of one- and two-dimensional high-resolution ^1H and ^{13}C NMR spectroscopy, ultraviolet and infrared spectroscopy, electron impact and liquid secondary ion mass spectrometry, and, in some cases, synthesis by an alternate route. Detailed ^{13}C NMR data for the parent compounds are presented for comparison purposes. These photoisomerization reactions take place cleanly in acetonitrile; the corresponding reactions occur in aqueous solution as well. For cytosine and 5-methylcytosine the photoreaction in acetonitrile is slow; however, the rate of reaction is greatly enhanced by N1 substitution. We determined the quantum yields for formation of the products derived from 2'-deoxycytidine to be 2.44×10^{-4} in water and 1.34×10^{-3} in acetonitrile. The mechanism of formation of the 3-ureidoacrylonitriles is proposed to involve initial formation of a N3–C6 Dewar structure, followed by a ring-opening rearrangement.

Introduction

Over the past 30 years, a significant amount of research effort has been devoted to determining the mechanisms by which absorption of ultraviolet (UV) light causes harmful effects on living tissues. It was clear early on that DNA is a primary cellular target of far-UV radiation; photochemical damage to DNA is believed to be an important contributor to UV-induced cell death, mutagenesis, and carcinogenesis.[1] Many studies concerning photoinduced reactions of nucleobases and related compounds have been published in efforts to identify the in vivo photoproducts responsible for these adverse effects.[1] A major breakthrough came with the isolation of the cyclobutane dimer of thymine by Beukers and Berends[2a] and Wang,[2b] which has since been isolated from the DNA of far-UV-irradiated cells[2c] and for which elaborate enzymatic repair mechanisms have been identified.[2d] Since then, a variety of other lesions involving DNA bases have been identified, including, for example, cytosine-derived cyclobutyl dimers,[3] pyrimidine hydrates,[4] and pyrimidine–pyrimidone photoconjugates.[5]

* To whom correspondence should be addressed.

(1) A series of extensive reviews in this area is provided in: (a) Wang, S. Y., Ed. *Photochemistry and Photobiology of Nucleic Acids*; Academic Press: New York, 1976; Vols. I and II. More recent reviews are given in: (b) Cadet, J.; Voituriez, L.; Grand, A.; Hruska, F. E.; Vigny P.; Kan, L-S. *Biochimie* **1985**, *62*, 277–292. (c) Hélène, C. In *From Photophysics to Photobiology*; Favre, A., Tyrrell, R., Cadet, J. Eds.; Elsevier: Amsterdam 1987; pp 3–22. (d) Peak, M. J.; Peak, J. G. *Photodermatology* **1989**, *6*, 1–15. (e) Smith, K. C., Ed. *Aging, Carcinogenesis, and Radiation Biology: The Role of Nucleic Acid Addition Reactions*; Plenum Press: New York, 1976.

(2) (a) Beukers, R.; Berends, W. *Biochim. Biophys. Acta* **1960**, *41*, 550–551. (b) Wang, S. Y., *Nature* **1960**, *188*, 844–846. (c) Patrick, M. H.; Rahn, R. O. In Reference 1a, Vol II, p 35 and references therein. (d) Friedberg, E. C. *DNA Repair*; W. H. Freeman: New York, 1985 and references therein.

(3) Fisher, G. J.; Johns, H. E. In Reference 1a, Vol. I, p 225 and references therein.

0002-7863/90/1512-7736$02.50/0